ACS central science

Research Article

Cite This: ACS Cent. Sci. 2019, 5, 1937−1945

http://pubs.acs.org/journal/acscii

Rational Design of a P2-Type Spherical Layered Oxide Cathode for High-Performance Sodium-Ion Batteries

Jun Xiao,[†] Fan Zhang,[‡] Kaikai Tang,[†] Xiao Li,[†] Dandan Wang,[†] Yong Wang,*[,†] Hao Liu,*[,†,‡] Minghong Wu,*[,†] and Guoxiu Wang*[,‡]

[†]Joint International Laboratory on Environmental and Energy Frontier Materials, School of Environmental and Chemical Engineering, Shanghai University, Shanghai 200444, China

[‡]Centre for Clean Energy Technology, School of Mathematical and Physical Sciences, Faculty of Science, University of Technology Sydney, Broadway, Sydney, New South Wales 2007, Australia

Supporting Information

ABSTRACT: Sodium-ion batteries (SIBs) have been regarded as the most promising candidates for the next-generation energy storage devices owing to their low price and high abundance. However, the development of SIBs is mainly hindered by the instability of cathode materials. Here, we report a new P2-type manganese-rich cathode material, $Na_{0.66}Li_{0.18}Mn_{0.71}Mg_{0.21}Co_{0.08}O_2$ (P2-NaLiMMCO) with uniform spherical structure prepared via a simple solvothermal method and subsequent solid-state reaction. This P2-NaLiMMCO cathode material with uniform microsize secondary spheres and nanosize primary crystalline particles delivers a high initial discharge capacity of 166 mA h g^{-1} and superior capacity retention, which are superior to most previously reported results. The improved stability of the cathode material was further investigated by the *in situ* X-ray diffraction technique, which suggests an enhanced reversibility of the cathode material during the desodiation/sodiation process. With the superior electrochemical performance and stable structures, this new P2-NaLiMMCO can serve as a practical cathode material for SIBs.

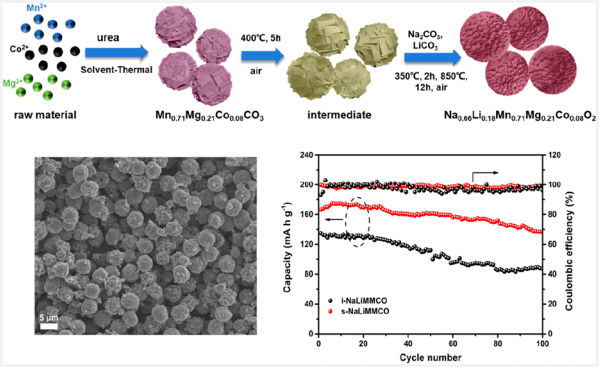

INTRODUCTION

Increasing attention has been paid to lithium-ion batteries (LIBs) due to the excessive consumption of fossil fuels and the need for sustainable development in the past decades. However, the deficiency of lithium resources makes LIBs insufficient for large-scale energy storage though they can provide high energy density. The rapidly growing demand for cheap and large energy storage systems has caused severe challenges regarding LIBs. Therefore, it is necessary to find an economic alternative to meet the increasing demand for large-scale energy storage.[1−4] In this aspect, as one of the alkali metal elements, sodium metal anode-based batteries (e.g., sodium-ion batteries, SIBs) have attracted great attention due to their similar electrochemical properties as compared to LIBs, low cost, and abundance.[5−9]

So far, there are still many intrinsic issues that limit the performance of existing cathode materials for SIBs. It is well-known that Na ions undergo a slower kinetic process than Li ions due to their larger ionic size (Na^+, 1.02 Å vs Li^+, 0.76 Å), which makes Na ions intrinsically difficult for the intercalation/deintercalation. What is worse, the structure of the host cathode material will collapse gradually along repeated insertion/extraction of large Na ions, which leads to a short battery life span and poor rate capabilities.[10,11] In order to resolve these problems, many cathode materials, such as metal oxides, polyanions, and so on, have been intensively investigated.[12−15] Among these above-mentioned cathodes, layered metal oxides (Na_xMO_2, M = transition metals) have attracted more attention because of the simple synthesis method as well as excellent electrochemical properties such as preferable specific capacity and good cycle life.[6,11,16,17] There are two major groups for Na_xMO_2, including O-type and P-type, which are classified by the oxygen stacking order. According to the previous literature, P2 and O3 cathode materials have caught more interest.[14,18] The O3 structure can provide high specific capacity with higher Na content, but it suffers from inferior cycle stability because of the slab-gliding during the charge/discharge process, resulting in structure collapse of the host material.[19,20] This shortcoming greatly limits its further application. In contrast, the P2 phase has larger layer spacing, which leads to rapid Na^+ diffusion without structure damage, exhibiting better cycle stability, though the initial specific capacity is slightly lower than O3 type.[21,22]

Many metal oxides with P2 phase, such as $Na_{0.5}Ni_{0.23}Fe_{0.13}Mn_{0.63}O_2$,[23] $Na_{2/3}Mn_{1/2}Fe_{1/4}Co_{1/4}O_2$,[24] $Na_{0.55}[Ni_{0.1}Fe_{0.1}Mn_{0.8}]O_2$,[25] $Na_{7/9}Cu_{2/9}Fe_{1/9}Mn_{2/3}O_2$,[26] and $Na_{0.66}Co_{0.22}Mn_{0.44}Ti_{0.34}O_2$,[27] have been explored and per-

Received: September 28, 2019
Published: December 6, 2019

DOI: 10.1021/acscentsci.9b00982
ACS Cent. Sci. 2019, 5, 1937−1945

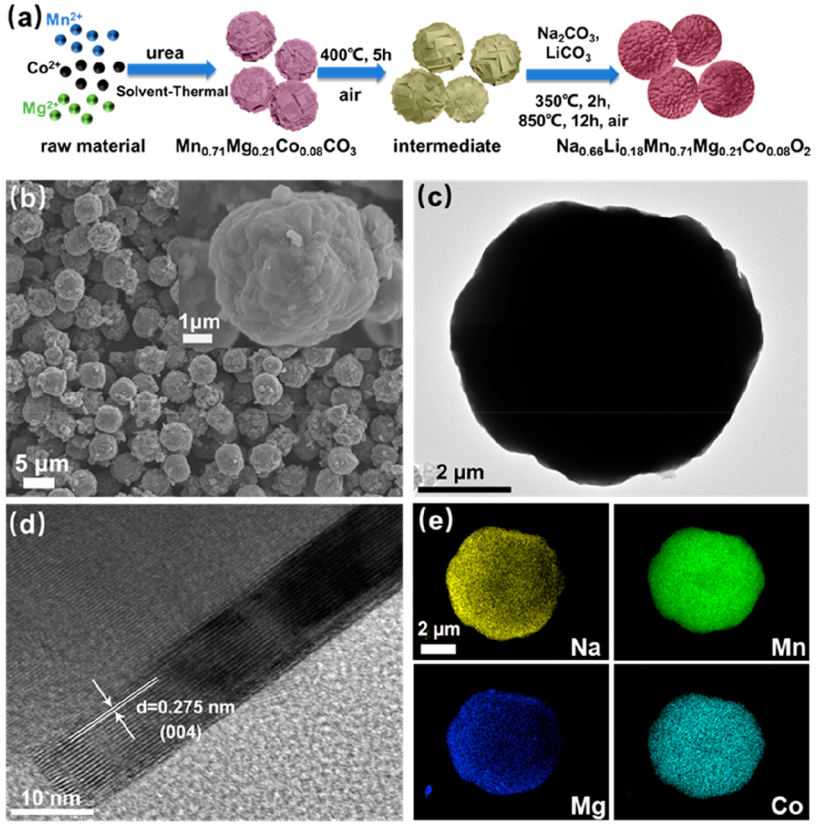

Figure 1. (a) Schematic diagram of the preparation processes of s-NaLiMMCO. (b) SEM images of the as-prepared s-NaLiMMCO. (c) Typical TEM image of s-NaLiMMCO. (d) HR-TEM image of s-NaLiMMCO. (e) EDS mapping images of sodium, manganese, magnesium, and cobalt. The inset is the corresponding SEM image with high magnification.

formed as cathode electrodes for SIBs. For instance, Xiao et al. developed a $Na_{2/3}Ni_{1/6}Mn_{2/3}Cu_{1/9}Mg_{1/18}O_2$ material composed of nanoflakes, which provides 87.9 mA h g^{-1} at a low rate of 0.5 C.[28] Fang et al. synthesized a novel $Na_{0.86}Co_{0.475}Mn_{0.475}Ti_{0.05}O_2$ cathode material through a simple solid-state method, showing improved stability during the sodium insertion/extraction process. This material only shows very low capacity decay after long cycling.[29] Li et al. reported a P2-$Na_{0.67}Mn_{0.65}Ni_{0.2}Co_{0.15}O_2$ material, which exhibited a superior capacity of 155 mA h g^{-1} when cycled at 12 mA g^{-1} and an excellent rate performance even when cycled at high rate density.[30] Many previous research results indicate that doping with Li, Zn, Mg, Al, and so on can greatly ameliorate the electrochemical properties of the original cathodes. For instance, researchers selected Li and Mg for doping due to their environmental friendliness and earth-abundance while the Co-substitution can improve conductivity. To be more specific, cation doping can effectively inhibit the Jahn−Teller effect of the Mn ion, promote the disorder of Na^+, and accelerate the kinetics of Na^+, thereby enhancing cycle life as well as rate performance.[16,21,31,32] Although some progress has been made in the research of the positive electrode material, there are still many challenges in developing a cathode electrode material which has excellent cycle stability and rate performance at the same time up to now.[14,32−34] Designing positive materials with a regular morphology is an effective way to boost sodium-ion storage. The augmented electrochemical properties are closely associated with the structure of the material, because a rationally designed structure such as a microspherical structure can enhance the reaction dynamics, reduce the side reactions of active material with electrolyte, and provide a higher tap density, thereby improving the energy density for practical applications.[35,36] Therefore, it is critical to synthesize a material with unique features with enhanced electrochemical performance for SIBs.

Herein, we prepared a novel Mn-rich P2-$Na_{0.66}Li_{0.18}Mn_{0.71}Mg_{0.21}Co_{0.08}O_2$ (denoted as P2-NaLiMMCO) microsphere material assembled by nanosized primary particles, via a modified solvothermal method and subsequent solid-state reaction. This P2-NaLiMMCO delivers a high initial discharge capacity of 166 mA h g^{-1} accompanied by a superior capacity retention of 82% after 100 cycles when cycled at a current of 20 mA g^{-1}. In addition, it also exhibits high Coulombic efficiency. *In situ* X-ray diffraction (XRD) investigation proves that the improved electrochemical properties are ascribed to the stable spherical structure, which can effectively suppress side reactions and alleviate the volume changes caused by sodium insertion/extraction, while small particles can shorten the transport pathway for Na ions, consequently boosting the performance of P2-NaLiMMCO.

RESULTS AND DISCUSSION

Figure 1a presents the schematic diagram of the preparation processes of P2-$Na_{0.66}Li_{0.18}Mn_{0.71}Mg_{0.21}Co_{0.08}O_2$ with a spherical structure (denoted as s-NaLiMMCO). The structure of the as-prepared s-NaLiMMCO sample is depicted in Figure 1b, which shows a globular structure with an average diameter of 3−6 μm composed of small primary particles. In addition, the precursor microspheres synthesized via a modified solvothermal method are shown in Figure S1a, made up of

DOI: 10.1021/acscentsci.9b00982
ACS Cent. Sci. 2019, 5, 1937−1945

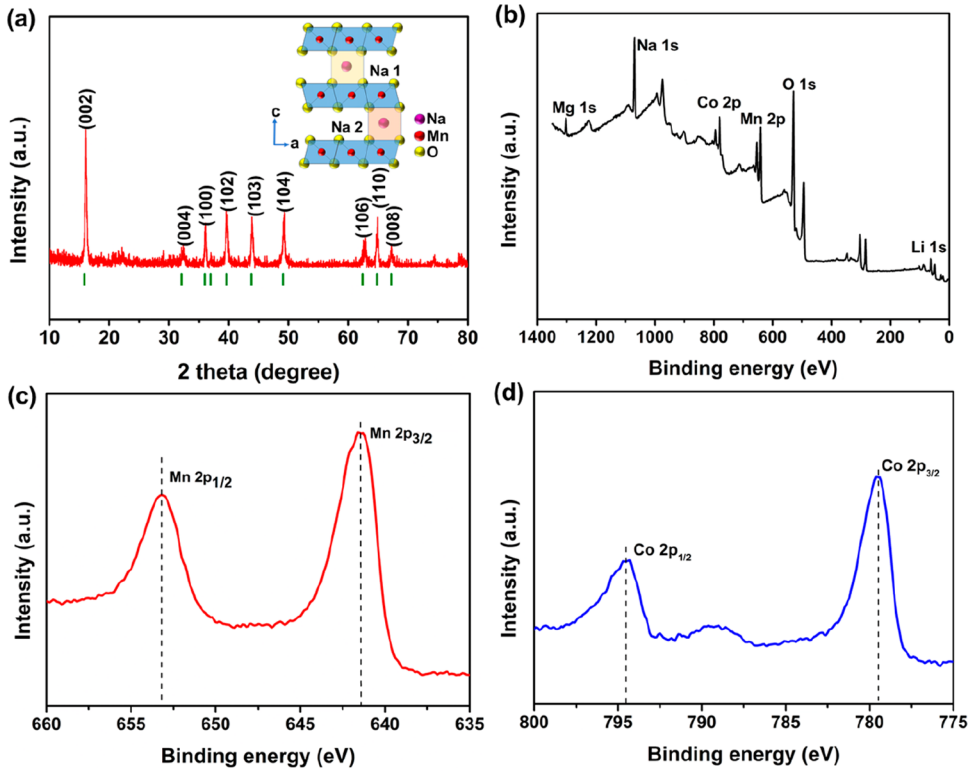

Figure 2. (a) X-ray diffraction data of the as-synthesized s-NaLiMMCO. The inset is the structure diagram of the P2 phase. (b) XPS spectra of s-NaLiMMCO. (c) High-resolution XPS spectra of Mn 2p. (d) High-resolution XPS spectra of Co 2p.

thin layers with a sharp edge. The heat treatment at 400 °C in air to remove organic residues of the intermediate does not change the morphology of precursor microspheres (Figure S1b). Transmission electron microscopy (TEM) further verifies the structure details of s-NaLiMMCO, as shown in Figure 1c–e. The TEM image demonstrates a microspherical structure and highly crystalline state for s-NaLiMMCO. Meanwhile, the *d*-spacing of clear adjacent lattice spacing shown in the high-resolution TEM (HR-TEM) image is 0.275 nm, corresponding to the (004) planes of P2-type s-NaLiMMCO (Figure 1d). EDS mapping images in Figure 1e suggest that Na, Mn, Mg, and Co elements are uniformly distributed on the s-NaLiMMCO microsphere, indicating that the solvothermal method is an effective method for preparing a spherical sample with a uniform element distribution, which is beneficial for Na^+ transmission due to the unique structure.

To prove the advantages of the spherical structure, P2-NaLiMMCO particles with an irregular shape have been prepared by coprecipitation method (denoted as i-NaLiMMCO). The synthetic details are described in the Experimental Section, and the size of i-NaLiMMCO bulk particles ranges from 1 to 2 μm, as presented in Figure S1c,d, which shows a larger exposed surface than s-NaLiMMCO. The XRD patterns of the precursor and intermediate are depicted in Figure S2a, which are isostructural with $MnCO_3$ (JCPDS 44-1472). In the hydrothermal process, urea decomposes under high temperature and high pressure to produce carbonate and hydroxide, which coprecipitate with transition metal ions to form primary particles. The primary particles subsequently aggregate to form spherical precursors.[37] According to the measurement results of ICP-OES, the ratios of each metal atom in the precursor and as-prepared sample are 0.7:0.20:0.08 and 0.65:0.18:0.69:0.20:0.07, respectively, consistent with the design expectation, as summarized in Tables S1 and S2.

Figure 2a exhibits the XRD pattern of s-NaLiMMCO. All Bragg diffraction peaks of the target product after high-temperature calcination are in good agreement with the pure P2 phase with a $P6_3/mmc$ space group (JCPDS 27-0751), showing that lithium and magnesium doping does not change the crystal structure of the original Mn-based material, which is similar to the article reported previously as well as the i-NaLiMMCO (Figure S2b).[38] In addition, the BET surface areas of s-NaLiMMCO and i-NaLiMMCO are 5.198 and 9.833 $m^2\ g^{-1}$ (Figure S3a,b), respectively. These results indicate that the contact area between s-NaLiMMCO and electrolyte is smaller, which can effectively reduce the side reactions with electrolyte, thus improving cycle stability. Moreover, there is no impurity that exists in the highly crystalline s-NaLiMMCO sample. The structure diagram of the metal oxide cathode material with P2 phase is depicted in the inset figure of Figure 2a, suggesting that the oxygen layers are stacked in accordance with the ABBA sequence, and sodium ions occupy the prismatic position. Meanwhile, sodium ions can be divided into Na_e and Na_f due to their located positions, which share the edges and faces with the transition metal octahedral, respectively.[29,39] For s-NaLiMMCO, transition metals locate in oxygen layers while Li occupies part of the sodium position.[38] The valence states of the transition metals in s-NaLiMMCO obtained by XPS measurement are depicted in Figure 2b–d. Figure 2b displays the states of all elements in a full spectrum survey. Particularly, Figure 2c presents the results of Mn 2p; the dominating binding energy peaks which are assigned to Mn $2p_{3/2}$ and Mn $2p_{1/2}$ are situated at 641.5 and 653.1 eV, indicating that Mn^{3+} and Mn^{4+} coexist in this material. This is consistent with the literature reported previously.[40,41] Figure

DOI: 10.1021/acscentsci.9b00982
ACS Cent. Sci. 2019, 5, 1937–1945

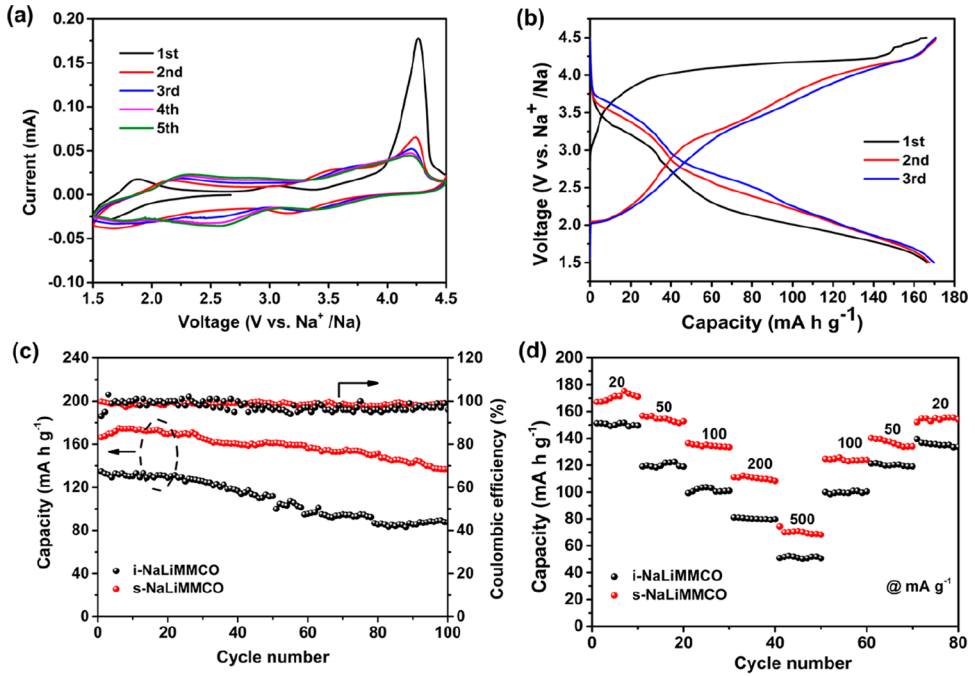

Figure 3. Electrochemical properties of the P2-NaLiMMCO cathode material. (a) Initial five CV profiles of the s-NaLiMMCO electrode at 0.1 mV s^{-1}. (b) Initial typical charge/discharge curves of s-NaLiMMCO at 20 mA g^{-1} between 1.5 and 4.5 V. (c) Cycling performance of s-NaLiMMCO and i-NaLiMMCO with the Coulombic efficiency at 20 mA g^{-1}. (d) Rate capacities of s-NaLiMMCO and i-NaLiMMCO material at different current densities.

2d illustrates that the two peaks of Co 2p which belong to $2p_{3/2}$ and $2p_{1/2}$ are at 779.5 and 794.6 eV, respectively, manifesting the existence of Co^{3+} in s-NaLiMMCO.[42]

The above-mentioned characterizations prove that the spherical Mn-based oxide with rational doping was successfully obtained. The as-prepared material has many advantages as a cathode material for SIBs due to its unique features. For example, the secondary spherical structure enables a high tap density so that an improved energy density can be achieved. Furthermore, the nanosized primary particles allow sodium diffusion dynamics in the solid state of s-NaLiMMCO. The multidoping can stabilize the crystal structure during charge/discharge processes owing to the difference of ionic deformation among all metal elements. All of these properties imply that the as-prepared s-NaLiMMCO has great potential to be a promising cathode material for SIBs.

Figure 3a displays the initial five CV curves of the s-NaLiMMCO cathode, which is scanned at the 0.1 mV s^{-1} rate between 1.5 and 4.5 V, exhibiting good stability and reversibility except for this first cycle. The redox peak at the low-voltage region of about 2.0 V comes down to a redox process of Mn^{3+}/Mn^{4+}. The redox peak at the high-voltage region is possibly related to the reversible oxidation/reduction reaction of cobalt.[38,42] The strong anodic peak at about 4.25 V during the incipient cycle is possibly related to the conclusion that a solid electrolyte interface (SEI) film is coming into being, and a high consistency of CV curves demonstrates the stability of the material during the electrochemical process after the initial activation cycle. A suitable electrolyte may do this material a favor by further improving the electrochemical properties, because it can help reduce parasite reactions referring to the active material and electrolyte ingredient.

The initial three charge−discharge curves of the s-NaLiMMCO cathode are revealed in Figure 3b, which were performed between 1.5 and 4.5 V at 20 mA g^{-1} with an open-circuit close to 2.8 V versus Na^+/Na. In the initial charge process, a slope from 2.8 to 4.0 V and a voltage platform at about 4.2 V are displayed, which are consistent with the CV result. The initial discharge capacity of s-NaLiMMCO is 166 mA h g^{-1} during the first discharge cycle accompanied by two slopes located at 4.5−2.8 and 2.8−1.5 V, respectively. Furthermore, the charge and discharge curves are identical in the following cycles. During subsequent cycles, higher overpotential can be found because of the high stress caused by the initial charge activation, indicating the high reversibility of the reaction during the Na^+ intercalation/deintercalation process after the first cycle. In the meantime, the voltage plateaus in charge and discharge curves are well matched with their CV curves. It can still provide a high capacity retention of ca. 82% after 100 charge/discharge processes, corresponding to the specific capacity of 136 mA h g^{-1}, while i-NaLiMMCO can only provide 65% capacity retention (Figure 3c). The s-NaLiMMCO experiences increasing capacity for the first several desodiation/sodiation cycles attributed to the activation process. Moreover, it provides a capacity decay of less than 0.2% per cycle during the first 100 cycles. The Coulombic efficiencies of the s-NaLiMMCO are higher than 97%. In contrast, the i-NaLiMMCO cathode displays poor properties, which delivers a lower initial capacity (~135 mA h g^{-1}) than the s-NaLiMMCO electrode and 80 mA h g^{-1} after 100 cycles. The microspherical structure not only increases the specific capacity of the P2-type NaLiMMCO material but also improves the cycle stability. It is apparent that the cycle stability of the s-NaLiMMCO cathode material at low current density is superior to many manganese-based materials with the P2 phase previously reported, as summarized in Table S3. A similar trend can be found in a higher charge/discharge rate (Figure S4), demonstrating that the s-NaLiMMCO has a

DOI: 10.1021/acscentsci.9b00982
ACS Cent. Sci. 2019, 5, 1937−1945

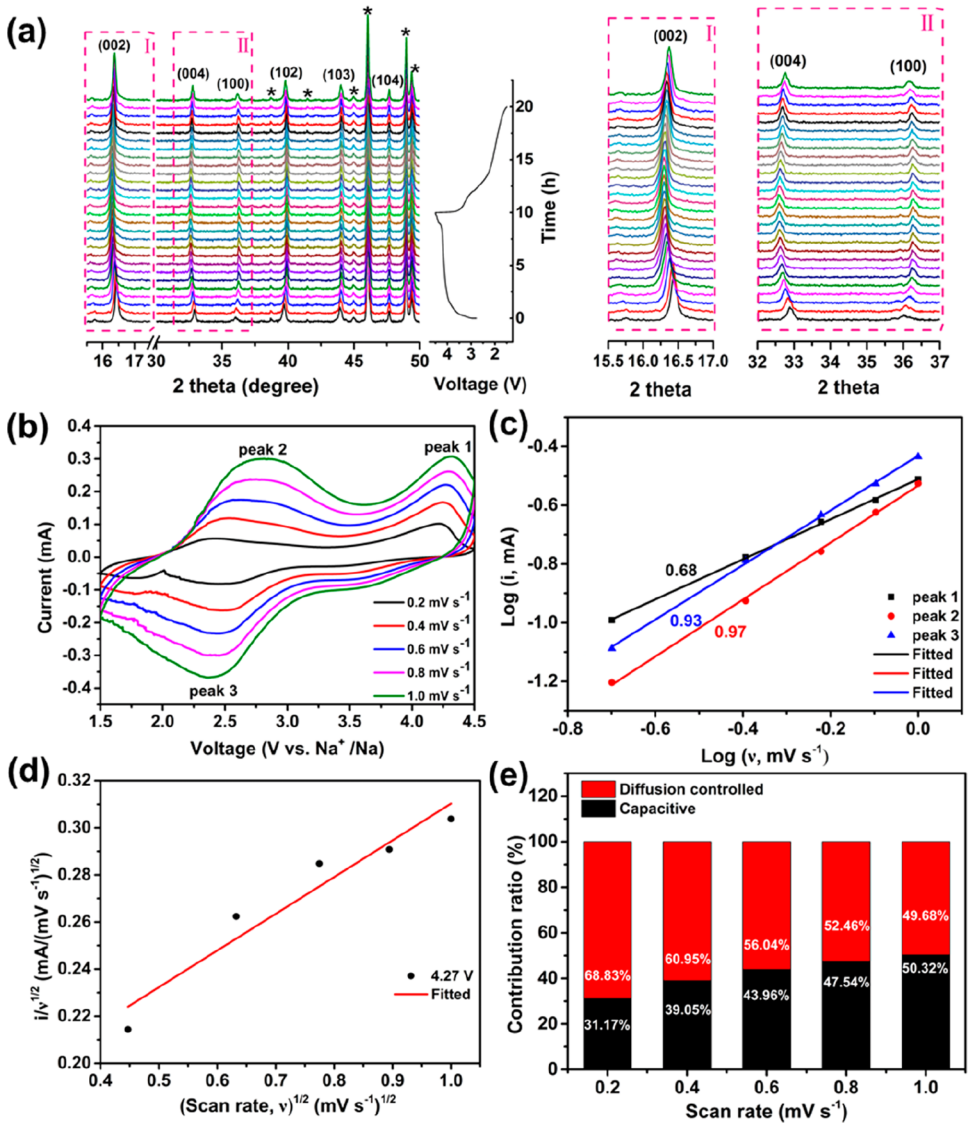

Figure 4. (a) *In situ* XRD patterns collected during the first charge/discharge process of the s-NaLiMMCO electrode between 1.5 and 4.5 V at the 0.1C rate. Black asterisks represent peaks of the Be window. (b) CV curves of the s-NaLiMMCO electrode at different scan rates ranging from 0.2 to 1.0 mV s^{-1}. (c) log(i) versus log(ν) plots. (d) $\nu^{1/2}$ versus $i/\nu^{1/2}$ plot used for calculating k_1 and k_2. (e) Contribution ratio of capacitive and diffusion-controlled behaviors at various scan rates.

better capacity retention. Figure S5a clearly reveals the outstanding cycle performance of the as-prepared s-NaLiMMCO material cycled at 100 mA g^{-1}. It is evident that the initial discharge capacity provided by this material is 128 mA h g^{-1} and a better retention than i-NaLiMMCO (Figure S5b).

The rate performances of the s-NaLiMMCO and i-NaLiMMCO electrode cycled at different current rate are depicted in Figure 3d, in which s-NaLiMMCO delivers 167.2, 154.7, 135.3, 110.8, and 70.8 mA h g^{-1}, at the current rate of 20, 50, 100, 200, and 500 mA g^{-1}, respectively. The P2-type s-NaLiMMCO cathode can still provide a high capacity of 155.5 mA h g^{-1}, when returning to the initial low rate, suggesting good reversibility over a wide range of rate densities. Figure S5c shows the charge/discharge curves at various rates. The excellent similarity proves the conclusion that s-NaLiMMCO is very stable at a high rate. For i-NaLiMMCO, the discharge capacity drops rapidly compared to s-NaLiMMCO from 151 mA h g^{-1} at the initial current (20 mA g^{-1}), and only a capacity of 50 mA h g^{-1} can be maintained when the current rate goes up to 500 mA g^{-1}. As the rate returns to 20 mA g^{-1}, the discharge capacity of i-NaLiMMCO only recovers to 134 mA h g^{-1}, suggesting a poor rate performance (Figure 3d and Figure S5d). The electrochemical improvements are attributed to the spherical structure and codoping of elements.

Layered metal oxides (Na_xMO_2) have the tendency to suffer from a P2−O2 phase transition due to sliding of the oxygen layers under low sodium conditions. Therefore, in order to study the phase transformation of the s-NaLiMMCO electrode in the electrochemical process, the *in situ* XRD investigation has been performed in the first charge−discharge cycle, as presented in Figure 4a. In the initial charging from 1.5 to 4.5 V, a typical (002) peak representing the P2 phase continuously shifted to a low angle without new peak formation, which indicates an expansion of the *c*-axis caused by the $O_2-O_2^-$ repulsion effect during the sodium extraction process. This is in good agreement with those CV curves in Figure 3a and charge−discharge profiles with slopes in Figure 3b, respectively. The intensity of the (002) peak hardly changes

DOI: 10.1021/acscentsci.9b00982
ACS Cent. Sci. 2019, 5, 1937−1945

throughout the process even when the battery is charged with a cutoff voltage up to 4.5 V, demonstrating that the structure is stable during the reaction process. When the cathode material is discharged to 1.5 V, the (002) peak gradually shifts to a high angle until it returns to the original state, suggesting the opposite change of *c*-axis versus charging process. The (004) peak undergoes the same process as the (002) peak, while the (100) peak goes through the reverse process, indicating that the *a*- and *b*-axes are decreasing when sodium is removed. Many materials undergo a phase change when charging to a high cutoff voltage; though the 2θ angle of the peaks of the material in this Article are slightly shifted, no peaks for the other phase appear, indicating that the P2 phase is maintained, further confirmed by the enlarged view of the (002), (004), and (100) peaks on the right side of Figure 4a. It is evident that the *in situ* XRD results prove that the stability of s-NaLiMMCO is enhanced, further demonstrating that codoping effectively inhibits the sliding of the transition metal layer and Jahn−Teller effect of the Mn ion caused by Na^+ extraction, thereby achieving improved cyclic properties.

The electrochemical impedance spectra (EIS) measurement has been carried out to investigate the kinetics and electrochemical performance of the s-NaLiMMCO material (Figure S6). The Nyquist plots consisting of semicircles and oblique lines, which are located at the high frequency region and low frequency region, are attributed to the charge transfer resistance (R_{ct}) and Warburg impedance of Na^+ diffusion during the sodium insertion/extraction process, respectively. As seen from Figure S6a, the cell with the s-NaLiMMCO electrode provides a small R_{ct} value of 280 Ω in the first cycle, and the value increases to about 320 Ω after 20 cycles, which facilitates sodium-ion transport during the charge and discharge process. However, the R_{ct} value provided by i-NaLiMMCO is much larger than that of s-NaLiMMCO (Figure S6b). The enhanced properties can be ascribed to the microspherical structure with uniform size and even distribution of this material, which shorten the diffusion path and improve conductivity.[37]

Moreover, the galvanostatic intermittent titration technique (GITT) has been used for determining the diffusion coefficient of Na^+ during the sodiation process. The GITT curves for s-NaLiMMCO and i-NaLiMMCO cathode materials are depicted in Figure S7a,b, respectively, which both show small polarization during the Na insertion process except the final state. The sodium diffusion coefficient (D_{Na^+}) can be calculated according to the simplified formula in the previously published literature:[43]

$$D_{Na^+} = \frac{4}{\pi\tau}\left(\frac{m_B V_M}{M_B A}\right)^2\left(\frac{\Delta E_S}{\Delta E_\tau}\right)^2 \quad (1)$$

Here m_B, M_B, and V_M are the loaded quality, molar mass, and molar volume of the P2-type NaLiMMCO active material. In addition, the V_M is supposed to be constant throughout the electrochemical process, and A is the contact area between the electrolyte and those as-prepared active materials. The value of D_{Na^+} calculated from obtained GITT data is shown in Figure S7c. It is obvious that the D_{Na^+} value of s-NaLiMMCO is greater than that of i-NaLiMMCO, which is consistent with the better electrochemical performance.

Furthermore, CV profiles tested at disparate sweep rates of 0.2, 0.4, 0.6, 0.8, and 1.0 mV s^{-1} have been measured to further illustrate the sodium storage mechanism of the P2-NaLiMMCO material. Figure 4b reveals that all the CV curves for s-NaLiMMCO show good similarity, which further proves the excellent reversibility of this material. The proportion of capacitance effects for P2-NaLiMMCO can be calculated from the equation between the peak current (i) and sweep rates (ν) as follows:[44]

$$i = a\nu^b \quad (2)$$

Parameter b which stands for the typical index of storage kinetics can be obtained by the plot between $\log(i)$ and $\log(\nu)$. When b is close to 0.5, it indicates that the reaction is governed by diffusion. Instead, when the value of b is close to 1.0, it indicates an electrochemical process controlled by capacitive behavior. For s-NaLiMMCO, the calculated b values for the three peaks selected in the CV curve are shown in Figure 4c. The slopes of the fitted curves for the two anodic peaks are 0.68 (peak 1) and 0.97 (peak 2), respectively, while the value of another cathodic peak is 0.93 (peak 3). It is obvious that diffusion-controlled behavior and the capacitance effect coexist in the s-NaLiMMCO electrode, and the capacitance contribution plays a dominating role at the low voltage region. The capacitance contribution can be acquired by the equation below:

$$i\,(\mathrm{V}) = k_1\nu + k_2\nu^{1/2} \quad (3)$$

in which $k_1\nu$ and $k_2\nu^{1/2}$ represent capacitance and diffusion contributions. Figure 4d shows the linear relationship between $\nu^{1/2}$ and $i/\nu^{1/2}$ which can be applied to calculate the k_1 and k_2 constants. Figure 4e reveals the proportion of capacitance contribution at different sweep rates, indicating that the ratio gradually increases as the sweep rate increases. The capacitance contribution in the s-NaLiMMCO electrode accounts for 31.17% when the cells are scanned at 0.2 mV s^{-1}, and the ratio increases to 50.32% when the sweep rate reaches 1.0 mV s^{-1}. Meanwhile, the high ratio occupied by the capacitance contribution at a high sweep rate comes from the fact that microsphere structure can provide plentiful paths for electron transfer, which is beneficial to enhance the electrochemical properties.

In general, s-NaLiMMCO microspheres can be successfully obtained and present excellent electrochemical properties for SIBs due to the following factors. First, the regular microspherical structure not only has a high tap density but also ensures a stable crystal structure, which can tolerate stress resulting from volume changes and accelerate Na^+ transmission during the sodiation and desodiation process. Second, due to the codoping of lithium and magnesium, the material undergoes a solid solution reaction mechanism even when operated at a high cutoff voltage of 4.5 V without an irreversible phase transition of P2−O2 that is very common in conventional manganese-based materials and unfavorable for electrochemical performance. Third, compared with i-NaLiMMCO, s-NaLiMMCO consisting of nanosized primary particles provides a small contact area of the material and electrolyte, which effectively suppresses the parasite reaction between the active material and electrolyte, thereby improving cycle stability and achieving high Coulombic efficiency. Last but not least, the s-NaLiMMCO microspheres consisting of smaller particles provide more sites for Na^+ transfer, shorten the diffusion distance, and improve transmission dynamics, thereby reducing the impedance during the sodiation/desodiation process. It even increases the contribution of capacitance in the material and causes an enhancement in

DOI: 10.1021/acscentsci.9b00982
ACS Cent. Sci. 2019, 5, 1937−1945

capacity. All contributions lead to excellent sodium storage properties of s-NaLiMMCO, including high specific capacity, excellent rate performance, and outstanding cycle stability, making it a potentially promising cathode material for sodium-ion batteries.

CONCLUSION

In summary, a layered P2-type $Na_{0.66}Li_{0.18}Mn_{0.71}Mg_{0.21}Co_{0.08}O_2$ material with a microspherical structure was synthesized via a facile modified solvothermal method followed by high-temperature calcination. The as-prepared material shows an excellent reversible capacity of 166 mA h g^{-1} accompanied with a superior capacity retention of 82% after 100 cycles when cycled at 20 mA g^{-1}. The improved electrochemical performance benefits from the microspherical structure, which can effectively alleviate the stress caused by the volume change during the sodiation and desodiation process as well as ameliorate electronic conductivity. In addition, small particles provide short pathways for Na^+ transport. The as-prepared $Na_{0.66}Li_{0.18}Mn_{0.71}Mg_{0.21}$ $Co_{0.08}O_2$ with uniform structure and enhanced performance can serve as a potential cathode material candidate for SIBs. This strategy may be capable of providing inspiration for the structural optimization of electrode materials for energy storage systems.

EXPERIMENTAL SECTION

Preparation of P2-$Na_{0.66}Li_{0.18}Mn_{0.71}Mg_{0.21}Co_{0.08}O_2$ Microspheres and Particles. The spherical precursor of $Mn_{0.71}Mg_{0.21}Co_{0.08}CO_3$ was first synthesized by the previously reported method.[33] In brief, 17.5 mL of water and 51.5 mL of glycerin were added to the beaker, and then, 3 g of urea, 0.562 g of $MnCl{\cdot}4H_2O$, 0.076 g of $CoCl_2{\cdot}6H_2O$, and 0.080 g of $MgCl_2$ were added to the above solution with vigorous magnetic stirring. The mixture was then put into a Teflon-lined stainless steel autoclave with a volume of 100 mL and heated at 180 °C in a drying oven for 12 h. The precursor microspheres were washed by centrifugation with ethanol and deionized water. The sample was then dried in a vacuum oven at 80 °C overnight, followed by a heat treatment at 400 °C for 5 h in an air atmosphere to remove organic residuals. The as-obtained intermediate was uniformly mixed with 0.148 g of Na_2CO_3 and 0.028 g of Li_2CO_3 in 2 mL of H_2O by sonication, and then, the mixture was dried to remove water. Finally, the dried mixture was calcined at 350 °C for 2 h and 850 °C for 12 h in an air atmosphere to obtain P2-$Na_{0.66}Li_{0.18}Mn_{0.71}Mg_{0.21}Co_{0.08}O_2$ microspheres. The resulting product was stored in an argon-filled glovebox to isolate water and air.

As a comparison, the P2-$Na_{0.66}Li_{0.18}Mn_{0.71}Mg_{0.21}Co_{0.08}O_2$ particles without a spherical structure were prepared by a straightforward coprecipitation approach. Certain amounts of $Mn(CH_3COO)_2{\cdot}4H_2O$ and $Co(CH_3COO)_2{\cdot}4H_2O$ were put into to a LiOH solution, and after stirring for 1 h, the precipitate powder was filtered and washed by deionized water several times. The dried precursor and Na_2CO_3, LiOH, and $Mg(OH)_2$ with a stoichiometric ratio were ground uniformly and then calcined at 500 °C for 4 h and 850 °C for 10 h in an air atmosphere to obtain a comparison product. The two experiments are safe, and no unexpected or unusually high safety hazards were encountered.

Materials Characterization. The morphology and energy-dispersive spectroscopy (EDS) of P2-$Na_{0.66}Li_{0.18}Mn_{0.71}Mg_{0.21}Co_{0.08}O_2$ were obtained through scanning electron microscopy (SEM, SU5000) and field-emission transmission electron microscopy (TEM, JEOL-2100F), respectively. The valence state of transition metals was determined by X-ray photoelectron spectroscopy (XPS, ESCALAB 250 Xi). Inductively coupled plasma optical emission spectrometry (ICP-OES, Optima 2100DV) was performed to obtain the atomic ratio of each metal element in the precursor and target product. The structure characteristic of target and comparison samples was obtained from X-ray diffraction (XRD, Rigaku D/MAX 2200VPC) using Cu Kα radiation in the 2θ range from 10° to 80°. The *in situ* XRD patterns of this cathode electrode were collected via a Swagelok cell, and the battery was cycled between 1.5 and 4.5 V at 0.1C.

Electrochemical Measurements. The as-prepared electrodes were made up of 60 wt % active material, 20 wt % acetylene black, and 20 wt % polyvinylidene fluoride (PVDF), which were coated onto the aluminum foil disks after mechanical mixing with solvent *N*-methyl-2-pyrrolidone (NMP), followed with an overnight drying process in a vacuum oven at 80 °C. Coin cells (CR2032-type) assembled for tests used sodium metal as the anode electrode and glass fiber as the separator, and the electrolyte consisted of a solution with 1.0 M $NaClO_4$ dissolved in a volume ratio of 1:1 ethylene carbonate (EC) and diethyl carbonate (DEC), as well as 5% FEC working as an additive. Charge/discharge measurements were conducted on a Neware CT-4008 battery test system between 1.5 and 4.5 V (vs Na^+/Na) at different rates. Cyclic voltammetry (CV) measurements were performed on a CHI660 electrochemical workstation in the potential range 1.5−4.5 V. Electrochemical impedance spectroscopy (EIS) tests were carried out in the frequency range between 100 kHz and 10 mHz.

ASSOCIATED CONTENT

Supporting Information

The Supporting Information is available free of charge at https://pubs.acs.org/doi/10.1021/acscentsci.9b00982.

Figures and tables for the target product (s-NaLiMMCO) and comparison sample (i-NaLiMMCO), including SEM, XRD, nitrogen sorption, electrochemical performance, electrochemical impedance spectra, GITT measurements, ICP analysis, and an electrochemical performance comparison with the previous literature (PDF)

AUTHOR INFORMATION

Corresponding Authors

*E-mail: yongwang@shu.edu.cn.
*E-mail: hao.liu@uts.edu.au.
*E-mail: mhwu@shu.edu.cn.
*E-mail: Guoxiu.Wang@uts.edu.au.

ORCID

Yong Wang: 0000-0003-3489-7672
Hao Liu: 0000-0003-0266-9472
Minghong Wu: 0000-0002-9776-671X
Guoxiu Wang: 0000-0003-4295-8578

Notes

The authors declare no competing financial interest.

DOI: 10.1021/acscentsci.9b00982
ACS Cent. Sci. 2019, 5, 1937−1945

■ ACKNOWLEDGMENTS

This project is financially supported by the Australian Research Council (ARC) through the ARC Discovery project (DP180102297) and Future Fellowship (FT180100705). Y.W. appreciates the support from Shanghai Science & Technology Committee (15520720600). All authors are thankful for the support from "Joint International Laboratory on Environmental and Energy Frontier Materials" and "Innovation Research Team of High-Level Local Universities in Shanghai".

■ REFERENCES

(1) Jo, C.-H.; Jo, J.-H.; Yashiro, H.; Kim, S.-J.; Sun, Y.-K.; Myung, S.-T. Bioinspired surface layer for the cathode material of high-energy-density sodium-ion batteries. *Adv. Energy Mater.* **2018**, *8*, 1702942.

(2) Yao, H. R.; Wang, P. F.; Gong, Y.; Zhang, J.; Yu, X.; Gu, L.; Yang, C. O.; Yin, Y. X.; Hu, E.; Yang, X. Q.; Stavitski, E.; Guo, Y. G.; Wan, L. J. Designing air-stable O3-type cathode materials by combined structure modulation for Na-ion batteries. *J. Am. Chem. Soc.* **2017**, *139*, 8440−8443.

(3) Kaliyappan, K.; Liu, J.; Xiao, B.; Lushington, A.; Li, R.; Sham, T.-K.; Sun, X. Enhanced performance of P2-$Na_{0.66}(Mn_{0.54}Co_{0.13}Ni_{0.13})O_2$ cathode for sodium-ion batteries by ultrathin metal oxide coatings via atomic layer deposition. *Adv. Funct. Mater.* **2017**, *27*, 1701870.

(4) Zhang, Y.; Wang, C.; Hou, H. S.; Zou, G. Q.; Ji, X. B. Nitrogen doped/carbon tuning yolk-like TiO_2 and its remarkable impact on sodium storage performances. *Adv. Energy Mater.* **2017**, *7*, 1600173.

(5) Wang, P. F.; Xin, H.; Zuo, T. T.; Li, Q.; Yang, X.; Yin, Y. X.; Gao, X.; Yu, X.; Guo, Y. G. An abnormal 3.7 V O3-type sodium-ion battery cathode. *Angew. Chem., Int. Ed.* **2018**, *57*, 8178−8183.

(6) Mu, L.; Xu, S.; Li, Y.; Hu, Y. S.; Li, H.; Chen, L.; Huang, X. Prototype sodium-ion batteries using an air-stable and Co/Ni-free O3-layered metal oxide cathode. *Adv. Mater.* **2015**, *27*, 6928−6933.

(7) Yang, J.; Han, D.-W.; Jo, M. R.; Song, K.; Kim, Y.-I.; Chou, S.-L.; Liu, H.-K.; Kang, Y.-M. $Na_3V_2(PO_4)_3$ particles partly embedded in carbon nanofibers with superb kinetics for ultra-high power sodium ion batteries. *J. Mater. Chem. A* **2015**, *3*, 1005−1009.

(8) Liu, H.; Liu, X. X.; Li, W.; Guo, X.; Wang, Y.; Wang, G. X.; Zhao, D. Y. Porous carbon composites for next generation rechargeable lithium batteries. *Adv. Energy Mater.* **2017**, *7*, 1700283.

(9) Nan, J. X.; Guo, X.; Xiao, J.; Li, X.; Chen, W. H.; Wu, W. J.; Liu, H.; Wang, Y.; Wu, M. H.; Wang, G. X. Nanoengineering of 2D mxene-based materials for energy storage applications. *Small* **2019**, *15*, 1902085.

(10) Xiao, Y.; Wang, P. F.; Yin, Y. X.; Zhu, Y. F.; Niu, Y. B.; Zhang, X. D.; Zhang, J.; Yu, X.; Guo, X. D.; Zhong, B. H.; Guo, Y. G. Exposing {010} active facets by multiple-layer oriented stacking nanosheets for high-performance capacitive sodium-ion oxide cathode. *Adv. Mater.* **2018**, *30*, 1803765.

(11) Hwang, J.-Y.; Myung, S.-T.; Yoon, C. S.; Kim, S.-S.; Aurbach, D.; Sun, Y.-K. Novel cathode materials for Na-ion batteries composed of spoke-like nanorods of $Na[Ni_{0.61}Co_{0.12}Mn_{0.27}]O_2$ assembled in spherical secondary particles. *Adv. Funct. Mater.* **2016**, *26*, 8083−8093.

(12) Zhang, J.; Fang, Y.; Xiao, L.; Qian, J.; Cao, Y.; Ai, X.; Yang, H. Graphene-scaffolded $Na_3V_2(PO_4)_3$ microsphere cathode with high rate capability and cycling stability for sodium ion batteries. *ACS Appl. Mater. Interfaces* **2017**, *9*, 7177−7184.

(13) Mao, J.; Luo, C.; Gao, T.; Fan, X.; Wang, C. Scalable synthesis of $Na_3V_2(PO_4)_3$/C porous hollow spheres as a cathode for Na-ion batteries. *J. Mater. Chem. A* **2015**, *3*, 10378−10385.

(14) Konarov, A.; Jo, J. H.; Choi, J. U.; Bakenov, Z.; Yashiro, H.; Kim, J.; Myung, S.-T. Exceptionally highly stable cycling performance and facile oxygen-redox of manganese-based cathode materials for rechargeable sodium batteries. *Nano Energy* **2019**, *59*, 197−206.

(15) Jiang, Y.; Yang, Z. Z.; Li, W. H.; Zeng, L. C.; Pan, F. S.; Wang, M.; Wei, X.; Hu, G. T.; Gu, L.; Yu, Y. Nanoconfined carbon-coated $Na_3V_2(PO_4)_3$ particles in mesoporous carbon enabling ultralong cycle life for sodium-ion batteries. *Adv. Energy Mater.* **2015**, *5*, 1402104.

(16) Bianchini, M.; Gonzalo, E.; Drewett, N. E.; Ortiz-Vitoriano, N.; López del Amo, J. M.; Bonilla, F. J.; Acebedo, B.; Rojo, T. Layered P2−O3 sodium-ion cathodes derived from earth abundant elements. *J. Mater. Chem. A* **2018**, *6*, 3552−3559.

(17) Jo, J. H.; Choi, J. U.; Konarov, A.; Yashiro, H.; Yuan, S.; Shi, L.; Sun, Y.-K.; Myung, S.-T. Sodium-ion batteries: building effective layered cathode materials with long-term cycling by modifying the surface via sodium phosphate. *Adv. Funct. Mater.* **2018**, *28*, 1705968.

(18) Ma, C.; Alvarado, J.; Xu, J.; Clement, R. J.; Kodur, M.; Tong, W.; Grey, C. P.; Meng, Y. S. Exploring oxygen activity in the high energy P2-type $Na_{0.78}Ni_{0.23}Mn_{0.69}O_2$ cathode material for Na-ion batteries. *J. Am. Chem. Soc.* **2017**, *139*, 4835−4845.

(19) Cao, M.-H.; Wang, Y.; Shadike, Z.; Yue, J.-L.; Hu, E.; Bak, S.-M.; Zhou, Y.-N.; Yang, X.-Q.; Fu, Z.-W. Suppressing the chromium disproportionation reaction in O3-type layered cathode materials for high capacity sodium-ion batteries. *J. Mater. Chem. A* **2017**, *5*, 5442−5448.

(20) Wang, P. F.; Yao, H. R.; Liu, X. Y.; Zhang, J. N.; Gu, L.; Yu, X. Q.; Yin, Y. X.; Guo, Y. G. Ti-substituted $NaNi_{0.5}Mn_{0.5-x}Ti_xO_2$ cathodes with reversible O3-P3 phase transition for high-performance sodium-ion batteries. *Adv. Mater.* **2017**, *29*, 1700210.

(21) Hou, P.; Li, F.; Wang, Y.; Yin, J.; Xu, X. Mitigating the P2-O2 phase transition of high-voltage P2-$Na_{2/3}[Ni_{1/3}Mn_{2/3}]O_2$ cathodes by cobalt gradient substitution for high-rate sodium-ion batteries. *J. Mater. Chem. A* **2019**, *7*, 4705−4713.

(22) Xu, S.; Wu, J.; Hu, E.; Li, Q.; Zhang, J.; Wang, Y.; Stavitski, E.; Jiang, L.; Rong, X.; Yu, X.; Yang, W.; Yang, X.-Q.; Chen, L.; Hu, Y.-S. Suppressing the voltage decay of low-cost P2-type iron-based cathode materials for sodium-ion batteries. *J. Mater. Chem. A* **2018**, *6*, 20795−20803.

(23) Hasa, I.; Buchholz, D.; Passerini, S.; Scrosati, B.; Hassoun, J. High performance $Na_{0.5}[Ni_{0.23}Fe_{0.13}Mn_{0.63}]O_2$ cathode for sodium-ion batteries. *Adv. Energy Mater.* **2014**, *4*, 1400083.

(24) Liu, L.; Li, X.; Bo, S.-H.; Wang, Y.; Chen, H.; Twu, N.; Wu, D.; Ceder, G. High-performance P2-type $Na_{2/3}(Mn_{1/2}Fe_{1/4}Co_{1/4})O_2$ cathode material with superior rate capability for Na-ion batteries. *Adv. Energy Mater.* **2015**, *5*, 1500944.

(25) Hwang, J. Y.; Kim, J.; Yu, T. Y.; Sun, Y. K. A new P2-type layered oxide cathode with extremely high energy density for sodium-ion batteries. *Adv. Energy Mater.* **2019**, *9*, 1803346.

(26) Li, Y.; Yang, Z.; Xu, S.; Mu, L.; Gu, L.; Hu, Y. S.; Li, H.; Chen, L. Air-stable copper-based P2-$Na_{7/9}Cu_{2/9}Fe_{1/9}Mn_{2/3}O_2$ as a new positive electrode material for sodium-ion batteries. *Adv. Sci.* **2015**, *2*, 1500031.

(27) Wang, Q. C.; Hu, E.; Pan, Y.; Xiao, N.; Hong, F.; Fu, Z. W.; Wu, X. J.; Bak, S. M.; Yang, X. Q.; Zhou, Y. N. Utilizing Co^{2+}/Co^{3+} redox couple in P2-layered $Na_{0.66}Co_{0.22}Mn_{0.44}Ti_{0.34}O_2$ cathode for sodium-ion batteries. *Adv. Sci.* **2017**, *4*, 1700219.

(28) Xiao, Y.; Zhu, Y. F.; Yao, H. R.; Wang, P. F.; Zhang, X. D.; Li, H.; Yang, X.; Gu, L.; Li, Y. C.; Wang, T.; Yin, Y. X.; Guo, X. D.; Zhong, B. H.; Guo, Y. G. A stable layered oxide cathode material for high-performance sodium-ion battery. *Adv. Energy Mater.* **2019**, *9*, 1803978.

(29) Fang, T.; Guo, S.; Jiang, K.; Zhang, X.; Wang, D.; Feng, Y.; Zhang, X.; Wang, P.; He, P.; Zhou, H. Revealing the critical role of titanium in layered manganese-based oxides toward advanced sodium-ion batteries via a combined experimental and theoretical study. *Small Methods* **2019**, *3*, 1800183.

(30) Li, Z.-Y.; Gao, R.; Sun, L.; Hu, Z.; Liu, X. Designing an advanced P2-$Na_{0.67}Mn_{0.65}Ni_{0.2}Co_{0.15}O_2$ layered cathode material for Na-ion batteries. *J. Mater. Chem. A* **2015**, *3*, 16272−16278.

(31) Yan, Z. C.; Tang, L.; Huang, Y. Y.; Hua, W. B.; Wang, Y.; Liu, R.; Gu, Q. F.; Indris, S.; Chou, S. L.; Huang, Y. H.; Wu, M. H.; Dou, S. X. A hydrostable cathode material based on the layered P2@P3 composite that shows redox behavior for copper in high-rate and long-cycling sodium-ion batteries. *Angew. Chem., Int. Ed.* **2019**, *58*, 1412−1416.

DOI: 10.1021/acscentsci.9b00982
ACS Cent. Sci. 2019, 5, 1937−1945

(32) Tapia-Ruiz, N.; Dose, W. M.; Sharma, N.; Chen, H.; Heath, J.; Somerville, J. W.; Maitra, U.; Islam, M. S.; Bruce, P. G. High voltage structural evolution and enhanced Na-ion diffusion in P2-$Na_{2/3}Ni_{1/3-x}Mg_xMn_{2/3}O_2$ ($0 \leq x \leq 0.2$) cathodes from diffraction, electrochemical and ab initio studies. *Energy Environ. Sci.* **2018**, *11*, 1470−1479.
(33) Wang, P. F.; You, Y.; Yin, Y. X.; Wang, Y. S.; Wan, L. J.; Gu, L.; Guo, Y. G. Suppressing the P2-O2 phase transition of $Na_{0.67}Mn_{0.67}Ni_{0.33}O_2$ by magnesium substitution for improved sodium- ion batteries. *Angew. Chem., Int. Ed.* **2016**, *55*, 7445−7449.
(34) Clément, R. J.; Billaud, J.; Robert Armstrong, A.; Singh, G.; Rojo, T.; Bruce, P. G.; Grey, C. P. Structurally stable Mg-doped P2-$Na_{2/3}Mn_{1-y}Mg_yO_2$ sodium-ion battery cathodes with high rate performance: insights from electrochemical, NMR and diffraction studies. *Energy Environ. Sci.* **2016**, *9*, 3240−3251.
(35) Fang, Y. J.; Yu, X. Y.; Lou, X. W. A practical high-energy cathode for sodium-ion batteries based on uniform P2-$Na_{0.7}CoO_2$ microspheres. *Angew. Chem.* **2017**, *129*, 5895−5899.
(36) Hwang, J. Y.; Oh, S. M.; Myung, S. T.; Chung, K. Y.; Belharouak, I.; Sun, Y. K. Radially aligned hierarchical columnar structure as a cathode material for high energy density sodium-ion batteries. *Nat. Commun.* **2015**, *6*, 6865−6973.
(37) Kaliyappan, K.; Xaio, W.; Sham, T.-K.; Sun, X. High tap density Co and Ni containing P2-$Na_{0.66}MnO_2$ buckyballs: a promising high voltage cathode for stable sodium-ion batteries. *Adv. Funct. Mater.* **2018**, *28*, 1801898.
(38) Guo, S.; Liu, P.; Yu, H.; Zhu, Y.; Chen, M.; Ishida, M.; Zhou, H. A layered P2- and O3-type composite as a high-energy cathode for rechargeable sodium-ion batteries. *Angew. Chem., Int. Ed.* **2015**, *54*, 5894−5899.
(39) Zheng, X.; Li, P.; Zhu, H.; Rui, K.; Zhao, G.; Shu, J.; Xu, X.; Sun, W.; Dou, S. X. New insights into understanding the exceptional electrochemical performance of P2-type manganese-based layered oxide cathode for sodium ion batteries. *Energy Storage Mater.* **2018**, *15*, 257−265.
(40) Wang, L.; Sun, Y.-G.; Hu, L.-L.; Piao, J.-Y.; Guo, J.; Manthiram, A.; Ma, J.; Cao, A.-M. Copper-substituted $Na_{0.67}Ni_{0.3-x}Cu_xMn_{0.7}O_2$ cathode materials for sodium-ion batteries with suppressed P2−O2 phase transition. *J. Mater. Chem. A* **2017**, *5*, 8752−8761.
(41) Chen, T.; Liu, W.; Gao, H.; Zhuo, Y.; Hu, H.; Chen, A.; Zhang, J.; Yan, J.; Liu, K. A P2-type $Na_{0.44}Mn_{0.6}Ni_{0.3}Cu_{0.1}O_2$ cathode material with high energy density for sodium-ion batteries. *J. Mater. Chem. A* **2018**, *6*, 12582−12588.
(42) Zhu, Y. E.; Qi, X. G.; Chen, X. Q.; Zhou, X. L.; Zhang, X.; Wei, J. P.; Hu, Y. S.; Zhou, Z. A P2-$Na_{0.67}Co_{0.5}Mn_{0.5}O_2$ cathode material with excellent rate capability and cycling stability for sodium ion batteries. *J. Mater. Chem. A* **2016**, *4*, 11103−11109.
(43) Zhou, P.; Liu, X.; Weng, J.; Wang, L.; Wu, X.; Miao, Z.; Zhao, J.; Zhou, J.; Zhuo, S. Synthesis, structure, and electrochemical properties of O′3-type monoclinic $NaNi_{0.8}Co_{0.15}Al_{0.05}O_2$ cathode materials for sodium-ion batteries. *J. Mater. Chem. A* **2019**, *7*, 657−663.
(44) Mao, Y.; Chen, Y.; Qin, J.; Shi, C.; Liu, E.; Zhao, N. Capacitance controlled, hierarchical porous 3D ultra-thin carbon networks reinforced prussian blue for high performance Na-ion battery cathode. *Nano Energy* **2019**, *58*, 192−201.

DOI: 10.1021/acscentsci.9b00982
ACS Cent. Sci. 2019, 5, 1937−1945